Full Paper

Propellants, Explosives, Pyrotechnics

DOI: 10.1002/prep.201300104

Preparation of Nano-RDX by Evaporation Assisted Solvent–Antisolvent Interaction

Raj Kumar,[a] Prem F. Siril,*[a] and Pramod Soni[b]

Abstract: Nanoparticles of cyclotrimethylenetrinitramine (RDX) were prepared by a simple re-precipitation method using acetone as solvent and water as the antisolvent. The effect of changing experimental parameters such as ratio of solvent to antisolvent, temperature of antisolvent during injection and concentration of solution on particle size and morphology of RDX was systematically studied. The size of the particles was characterized using dynamic light scattering (DLS) and field emission scanning electron microscopy (FESEM). The mean particle size of the RDX nanoparticles according to FESEM analysis ranged from 40 nm to 230 nm under different conditions of preparation. The UV/Vis absorption maximum of nano-RDX was found to be blue shifted when compared to the absorption maximum for bulk-RDX. Powder X-ray diffraction (XRD) results showed that RDX nanoparticles precipitated in stable α-crystalline form. Fourier transform infrared (FTIR) spectroscopy was used to characterize the chemical nature of the nano-RDX. Thermal characterization of the RDX-nanoparticles was done using simultaneous thermogravimetric analysis coupled with differential scanning calorimetry (TGA-DSC).

Keywords: Nano-RDX · Solvent-antisolvent interaction · Evaporation-assisted precipitation · Spherical nanoparticles · Optical absorption

1 Introduction

Formation of small solid particles of micrometer or submicrometer size with controlled particle size distribution is of great interest in applications involving polymers, drugs and energetic materials [1]. In general, the aim of research and development activities in the area of high energy materials (HEMs) is focused on developing energetic materials with improved performance but with reduced sensitivity [2,3]. The focus of research in high explosives has been mainly to synthesize new explosive molecules with the above stated benign properties [4]. However, development through molecular modelling and organic synthesis of novel energetic materials has been very slow and conventional nitramine explosives such as RDX and HMX are still the most commonly used explosives across the globe. Powerful explosives such as CL-20 and octanitrocubane have higher energetic performance than HMX [3,4]. But, sensitivity to accidental stimuli is a matter of concern. The sensitivity of explosives is related to their chemical as well as physical characteristics [5]. Even though development in synthesis of new explosive molecules is small, physical properties such as crystal size, shape, morphology, purity, inclusions, defects in the crystal and the microstructure of inter-crystalline voids can be altered to improve the performance of existing explosives. Thus, crystal engineering offers some prospects for the improvement in performance of energetic materials by controlling some of these physical properties [6].

Theoretical models for the impact initiation of explosives indicate that the sensitivity to external stimuli decreases with decreasing crystal size [5,7]. Some experimental data also supports this theory [8–10]. In addition to significant reduction in sensitivity, novel behavior in deflagration to detonation transition was observed with submicrometer-sized particles. It is reported in the literature that nano-TATB crystals have higher mass loss than the micro-TATB crystals [11]. Thus, by size reduction of the crystals, sensitivity can be reduced and reactivity can be improved. A few studies have indicated that the particle size of explosives has influence on impact sensitivity and maximum energy output from a detonation [12,13].

However, only limited production strategies are available for making organic nanoparticles in general when compared to the large number of methods available for the preparation of inorganic nanoparticles. Methods used for the preparation of organic nanoparticles are primarily based on either precipitation, milling or through chemical reaction techniques [14]. Submicrometer-sized particles of energetic compounds have been prepared using various techniques such as sol-gel method [15], supercritical fluid methods [16,17], mechanical milling [18], ultrasonication

[a] *R. Kumar, P. F. Siril*
School of Basic Sciences, Indian Institute of Technology Mandi
Mandi-175001, Himachal Pradesh, India
Fax: +91-1905-237942
**e-mail: prem@iitmandi.ac.in*

[b] *P. Soni*
Terminal Ballistics Research Laboratory
Sector-30, Chandigarh-160030, India

[19–21], spray assisted precipitation [21,22], plasma enhanced crystallization [23] etc. There are relative advantages and disadvantages for all of these methods. For example, milling techniques rely on applying extremely high mechanical energy on the system leading to structural changes of the crystal [24]. Milling energetic materials can be hazardous also. Sol-gel methods are multi-step and time consuming synthetic routes [25]. As a consequence, methods which rely on solubility changes to induce nanoparticle formation are lately becoming attractive. Among these, reprecipitation is a simple and convenient technique, which proved to be particularly effective for the preparation of organic nanoparticle dispersion [24–26]. In this method, an organic solution containing an active substance is injected to the antisolvent (e.g. water) that is solvent-miscible under rapid mixing, which generates high supersaturation leading to fast nucleation rates. The instantaneous precipitation occurs by a rapid desolvation of the hydrophobic active ingredient in the antisolvent medium [26]. The precipitation rate can be enhanced by elevated temperatures during mixing and often such methods are called evaporation precipitation into aqueous solution (EPAS) [27,28]. The antisolvent may contain hydrophilic stabilizers such as polymers or surfactants. The hydrophilic stabilizer in the antisolvent is absorbed on the particle surface to inhibit particle growth. Herein, a simple solvent–antisolvent interaction method for the preparation of nano-RDX is reported.

2 Experimental Section

2.1 Materials

RDX was prepared in-house following the Bachmann procedure and was purified by repeated recrystallization [29]. Acetone was purchased from Sigma Aldrich and was used as received. Ultra-pure water (18.2 $M\Omega\,cm^{-1}$) from double stage water purifier (ELGA, PURELAB Option-R7) was used throughout. HPLC micro syringe was from Hamilton, USA. The disposable polystyrene cuvette was purchased from Sigma Aldrich, India. A syringe filter from Millipore, USA was used.

2.2 Preparation of RDX Nanoparticles

Accurately weighed RDX was dissolved in acetone to prepare a stock solution of 200 mM concentration. Dilute solutions of varying concentrations (5 mM, 10 mM, and 25 mM) were prepared by diluting the stock solution. The RDX solution (100 μL) was quickly injected to a fixed volume of water (25 mL) at constant temperature (30–70 °C) under magnetic stirring to produce the nanoparticles. Stirring was continued up to 2 min after injection. The RDX solution was always filtered using a syringe filter of pore size 0.1 μm before injection.

2.3 Particle Size Measurement and Characterization

Primary characterization of the particles (z-average diameter, d) and polydispersity index (Pdi) was measured using dynamic light scattering (DLS) (Zetasizer Nano ZS, Malvern Instrument Ltd., UK) at 25 °C. Pdi is a dimensionless parameter calculated from a simple two parameter fit to the correlation data in DLS. A smaller value of Pdi indicates that the sample is monodisperse. Pdi values lower than 0.7 are generally considered to be valid for DLS analysis of particle sizes. The instrument contains a 4 mW He–Ne laser operating at a wavelength of 633 nm and incorporates noninvasive backscatter optics (NIBS). The measurements were made at a detection angle of 173°. The sample containing polystyrene cuvette was placed in the temperature controlled chamber to maintain constant temperature.

Particle size and morphology of samples was also observed using an FESEM (FEI Quanta FEG 450). The suspension of RDX nanoparticles in water was drop-coated on a glass slide and dried. The dried sample was transferred onto a carbon tape applied on a clean SEM stub, which was subsequently sputter-coated with gold before the FESEM observations. The particle size of nano-RDX was calculated from FESEM images by averaging the diameter of at least 300 particles from images of different areas of the same sample.

The absorption spectra of the RDX nanoparticles dispersed in water were measured using a Shimadu double beam UV/Vis spectrophotometer, using a quartz cuvette in the wavelength range of 200 nm to 800 nm. Pure water was used as reference. FTIR spectroscopy was performed using Perkin–Elmer FTIR emission spectrometer (spectrum two). The FTIR spectrum of RDX nanoparticles was recorded from 4000–600 cm^{-1} frequency range with a resolution of 4 cm^{-1} and 8 scans. The sample was properly ground with KBr powder and then pressed to obtain a suitably sized pellet for FTIR spectrum recording. Pure KBr pellet was used for background correction. XRD patterns were recorded on a Smart Lab X-ray diffractometer (Rigaku, Japan) using Cu-K_α radiation as X-ray source ($\lambda = 0.15418$ nm), at room temperature. The voltage and current applied were 45 kV and 160 mA, respectively. The samples were placed in a glass sample holder and scanned from 2θ, 10° to 70° at a scan rate of 2° per min with a step size of 0.02°. TGA-DSC analyses were carried out by using a Netzsch STA 449 F1 Jupiter instrument. A small amount of the sample (2–3 mg) was kept in a standard alumina pan with an alumina lid with a pin hole at the middle. An empty crucible was used as reference. The samples were heated from room temperature to 500 °C at a heating rate of 5 $K\,min^{-1}$ under nitrogen atmosphere with a flow rate of 60 $mL\,min^{-1}$.

3 Results and Discussion

RDX is soluble in acetone up to 200 mM at room temperature. Injection of RDX solution in water immediately leads to the formation of nano-sized particles in DLS within a few minutes after the injection. However, no particles were visible with the naked eye probably due to the small size of the particles. RDX nanoparticles tend to aggregate and settle down over a period of time. This is obvious as no stabilizers were used. However, mild sonication was sufficient to re-disperse the aggregates. In order to optimize the preparation of nanoparticles with smaller particle size, narrow size distribution and relatively larger quantities, experimental conditions such as ratio of solvent to antisolvent, temperature of antisolvent during injection and concentration of solution were systematically varied. The particle size in each different condition was monitored using DLS and FESEM. The results are discussed in the following section.

3.1 Effect of Experimental Parameters on the Particle size of RDX

3.1.1 Effect of Ratio of Solvent to Antisolvent

The ratio of solvent to antisolvent was varied systematically by keeping the solvent volume constant (100 μL) and by varying the volume of antisolvent from 5 to 100 mL. The temperature of antisolvent was kept at 70 °C. The particle size was measured using dynamic light scattering (DLS) and the data is reported in Table 1.

It is evident from Table 1 that particle size decreased as the ratio of solvent to antisolvent was varied from 1:50 to 1:250. But at still higher ratios such as 1:500, particle size increased. Thus, 1:250 was found to be the optimum ratio. All further experiments were performed at this ratio. The Pdi values reported in Table 1 indicated that the nano-RDX samples were rather polydisperse.

3.1.2 Effect of Temperature and Concentration of the Antisolvent

The effect of temperature of the antisolvent during injection on the particle size was studied by varying temperature between 30 °C to 70 °C. The size of RDX nanoparticles that were formed at different temperatures as measured from DLS and FESEM is summarized in Table 2. Representative FESEM images are shown in Figure 1. The effect of concentration of the RDX solution in acetone on the particle

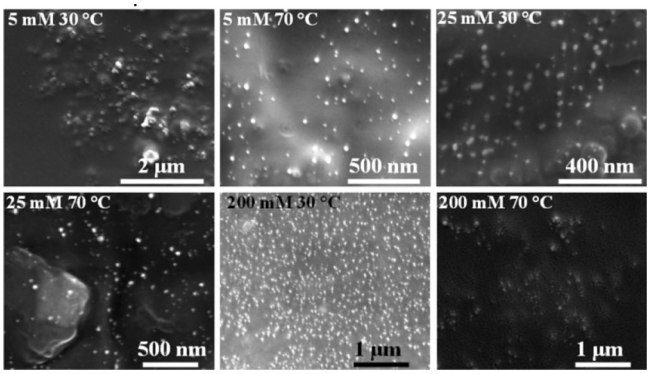

Figure 1. FESEM images of RDX nanoparticles. The experimental conditions (concentration of RDX in acetone and temperature of antisolvent during injection) of preparing them are inscribed on each image.

Table 1. Effect of varying the solvent to antisolvent ratio (v/v) on the particle size of nano-RDX.

Serial number	Volume of solvent [μL]	Volume of anti-solvent [mL]	Ratio of solvent to antisolvent	Particle size (d) [nm]	Pdi
1	100	5	1:50	372 ± 13	0.34 ± 0.06
2	100	10	1:100	393 ± 11	0.40 ± 0.05
4	100	25	1:250	238 ± 24	0.31 ± 0.07
5	100	50	1:500	311 ± 10	0.34 ± 0.04
6	100	100	1:1000	352 ± 36	0.41 ± 0.07

Table 2. Particle size variation of RDX nanoparticles with experimental variables such as temperature of anti solvent (T) and concentration of RDX solution.

T [°C]	Particles size (d) [nm]						
	5 mM		10 mM	25 mM		200 mM	
	DLS	SEM	DLS	DLS	SEM	DLS	SEM
30	322 ± 24	64 ± 35	312 ± 7	284 ± 18	85 ± 40	262 ± 29	229 ± 97
40	269 ± 7	–	305 ± 22	282 ± 24	–	264 ± 6	–
50	364 ± 20	–	289 ± 28	280 ± 29	–	262 ± 20	–
60	261 ± 2	–	290 ± 37	269 ± 34	–	239 ± 8	–
70	262 ± 27	38 ± 15	222 ± 14	232 ± 13	61 ± 27	216 ± 21	172 ± 66

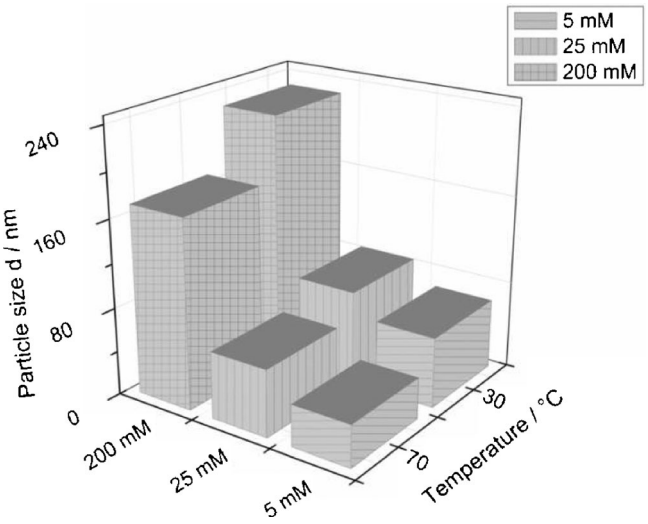

Figure 2. Three-dimensional plot of particles size of nano-RDX calculated from FESEM images against temperature of antisolvent and concentration of RDX solution in acetone.

size at different temperatures was also investigated and the corresponding data is also reported in Table 2.

A three-dimensional plot of the particle size (as measured from FESEM images) against temperature of antisolvent and concentration of RDX solution in acetone is shown in Figure 2. It is apparent from the data in Table 2, Figure 1 and Figure 2 that temperature of the antisolvent affects the particle size. Increasing the temperature of the antisolvent to 70 °C resulted in decreased particle size.

The mean particle size (z-average) calculated from DLS was found to be significantly higher than the mean diameter calculated from FESEM images. This may be due to a number of reasons. The presence of a small fraction of large sized particles can result in a higher z-average value in particle size measurement using DLS. Another reason could be aggregation of the nanoparticles in aqueous suspension as no stabilizing agent for the nanoparticles has been used. Again the presence of even a small amount of aggregates will result in higher z-average particle size. Although mostly individual nanoparticles without any aggregation in FESEM images (Figure 1) existed, aggregated particles were invariably observed, albeit in small numbers. Even for apparent aggregates of a small number of particles for which individuality of particles was clearly distinct in the FESEM images, the particle size of individual particles was estimated by calculating the average. Additionally, it has to be noted that FESEM imaging uses only a very small volume fraction of the sample and hence may be prone to sampling biases.

With all methods used for measuring the particle size, the general observation was that increasing the antisolvent temperature to 70 °C resulted in decreased particle size. The effect was strongly evident in the particle size that was measured from FESEM imaging. The average particle size measured by DLS method was under all conditions in the range of 320 nm to 215 nm. However, the average particle size that was measured from FESEM images ranged between 230 nm to 40 nm. The formation of particles with very small size at higher temperature can be explained because of the solvent evaporation at high temperatures. Evaporation rate of solvent is faster at high temperatures. Faster evaporation leads to quicker supersaturation, which in turn leads to greater nucleation [28]. Enhanced nucleation and the separation of nucleation and subsequent growth processes not only results in decreased particle size but also leads to uniform size of particles [28]. As the boiling point of solvent (acetone) is 56 °C, higher temperature of the antisolvent, especially at 70 °C, leads to evaporative re-precipitation resulting in smaller particle sizes. No experiments were performed below 70 °C owing to the difficulty in handling the experiment such as evaporation of the antisolvent.

The DLS data did not clearly reveal the effect of changing the concentration of RDX in acetone on particle size. However, it is apparent from FESEM data that the particle size increases as the concentration of RDX increases in acetone. At lower concentration (5 mM) the mean particle size was only 40 nm at 70 °C. However, average particle size increased to 170 nm, when the concentration was increased to 200 mM at 70 °C. The increase in particle size with increase in concentration of RDX in acetone is obvious. Because, although the supersaturation will be achieved at a faster rate when the concentration is high, there is enough supply of the precursor to sustain the growth of nuclei long enough so that the nuclei grow into relatively bigger particles. However, the ability to prepare particles in the nanometer length scales even at high concentration is required to prepare such nanoparticles in large quantities and this has been established by the reported method herein.

3.2 Characterization of Nano-RDX

The optical absorption of RDX nanoparticles dispersed in water with different experimental conditions was characterized by UV/Vis spectrophotometer. Absorption spectra of two representative samples are shown in Figure 3. Optical absorption spectrum of bulk-RDX particles suspended in water was also recorded for comparison and the data is also shown in Figure 3. Bulk-RDX showed an absorption peak at 240 nm. This is similar to the reported data [30]. However, the nano-RDX samples absorbed at 228 nm and 270 nm. The peak at 270 nm is due to the presence of acetone [31]. It is interesting to note that the absorption maxima for nano-RDX is blue shifted with reference to bulk-RDX. The reason for such size dependent shifting of absorption peaks for organic nanoparticles in general are usually different from that of inorganic nanoparticles. The blue shift of absorption maxima for nano-RDX may be due

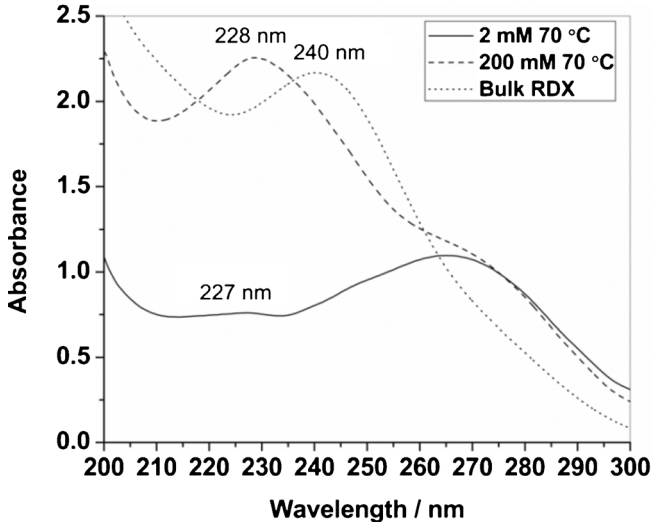

Figure 3. UV/Vis absorption spectra of bulk-RDX and nano-RDX samples suspended in water.

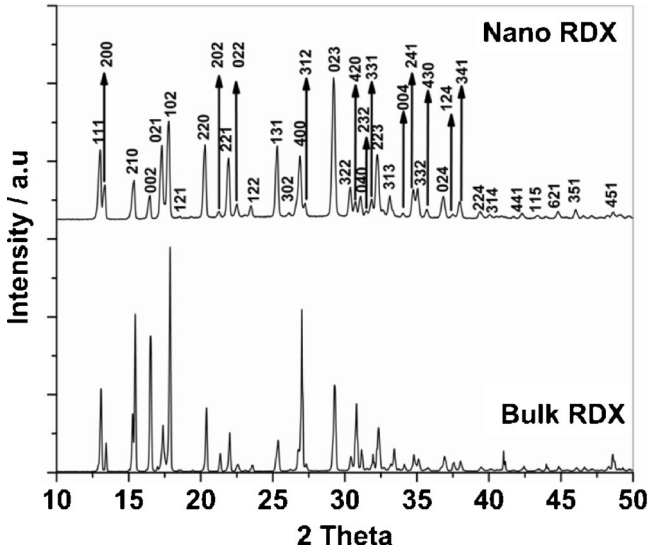

Figure 5. XRD patterns of bulk-RDX and nano-RDX prepared from 200 mM RDX solution in acetone with the antisolvent temperature at 70 °C.

to slight change in lattice state as a result of the increased surface area of the nanoparticles [32].

FTIR spectroscopy was used to determine the chemical composition before and after the antisolvent precipitation method. The FTIR spectrum of bulk-RDX is reported in Figure 4 along with the spectrum for one representative nano-RDX sample. It is clearly evident from Figure 4 that nano-RDX has similar IR bands to that for bulk-RDX. Major bands observed were similar to the bands that are reported in the literature [33]. The major bands can be assigned as follows: 1592 cm^{-1} (ν_s NO_2), 1270 cm^{-1} (ν_s $NO_2+\nu$ N–N), 1039 cm^{-1} (ring stretching bands), 945 cm^{-1}, and 783 cm^{-1} (δ NO_2 and γ NO_2) and 604 cm^{-1} ($\tau+\gamma$ NO_2) [34]. It can be

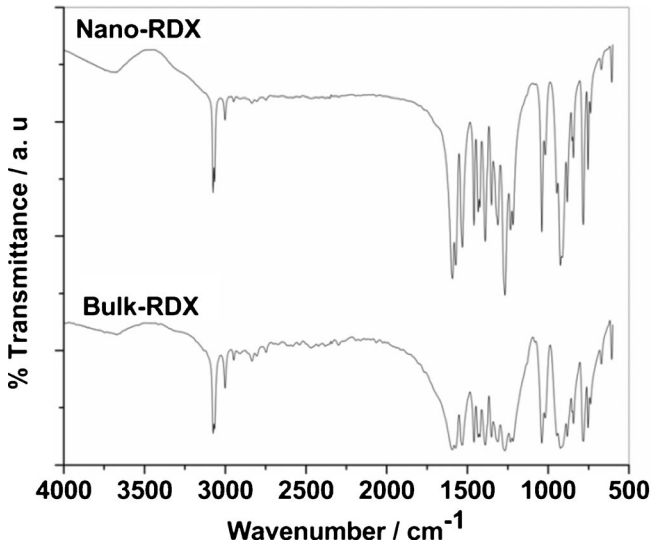

Figure 4. FTIR spectrum of bulk-RDX and nano-RDX prepared from 200 mM RDX solution in acetone with the antisolvent temperature at 70 °C.

concluded that antisolvent precipitation of RDX does not lead to any chemical modification of RDX even at elevated temperatures. Additionally, no band at 1720 cm^{-1} (ν_s CO) was observed, which clearly indicates the absence of any significant amount of residual acetone.

An XRD measurement was performed to ascertain the crystalline state of the nano-RDX. The XRD pattern of a representative nano-RDX sample is shown Figure 5 along with the diffraction pattern for bulk-RDX. The XRD pattern of the bulk-RDX and nano-RDX showed the presence of numerous distinct peaks showing the crystalline nature of the samples. The crystal structure of RDX is well known to have at least 5 different polymorphs: α, β, γ, δ and ε. The α-form is the most stable form at room temperature (orthorhombic, $a=1.3182$ nm, $b=1.1574$ nm, $c=1.0709$ nm) [35,36]. The diffraction pattern of bulk-RDX matched well with the α-form of RDX [37]. Major peaks are indexed in Figure 5. The RDX nanoparticles prepared also showed similar XRD pattern. This clearly indicates that RDX nanoparticles made by solvent antisolvent interaction are also in the α-form. Additionally, no effect of the experimental variables on the crystallinity of the nano-RDX samples produced by the solvent anti solvent interaction was observed.

Thermal characterization of nano-RDX samples was performed by using TGA-DSC. An overlay of TGA-DSC thermal curves of a representative nano-RDX sample is shown along with thermal curves of bulk-RDX sample in Figure 6. A sharp endothermic peak corresponding to melting of RDX was observed at 203.9 °C for bulk-RDX [38]. The nano-RDX melted at a slightly lower temperature, i.e. 202.8 °C. An additional endothermic peak along with a very small mass loss was observed for nano-RDX at around 52.6 °C. This may be due to the evaporation of residual acetone present

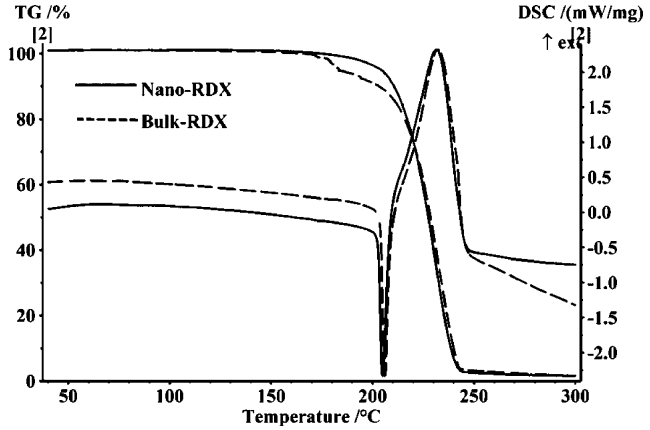

Figure 6. TGA-DSC thermal curves for bulk-RDX and nano-RDX. Samples were heated from room temperature to 500 °C at the rate of 5 K min^{-1} under nitrogen atmosphere.

in nano-RDX. A small mass loss was observed for bulk-RDX at around 180 °C in TGA thermal curve and a corresponding endotherm was observed in DSC. However, this feature was absent for nano-RDX. Mass loss in this temperature range is usually attributed to the sublimation of RDX [39]. Interestingly nano-RDX did not sublime, even though TGA-DSC analysis of it was performed under the same condition as bulk-RDX.

4 Conclusions

RDX was precipitated into nano-sized particles with spherical morphologies using evaporation assisted solvent anti-solvent precipitation method. High concentration of RDX solution favors the formation of relatively larger particles. Smaller nanoparticles were obtained when the anti solvent temperature was 70 °C when compared to lower temperatures. Nano-RDX precipitated in the stable α-crystalline form.

Acknowledgments

Thanks are due to AMRC, IIT Mandi for providing laboratory facilities. Financial assistance from ARMREB (DRDO), DST and UGC is gratefully acknowledged. CMSE, NIT Hamirpur is also thanked for FESEM imaging.

References

[1] L. E. Fried, M. R. Manaa, P. F. Pagoria, R. L. Simpson, Design and Synthesis of Energetic Materials, *Annu. Rev. Mater. Res.* **2001**, *31*, 291 – 321.
[2] G. Singh, I. P. S. Kapoor, S. K. Tiwari, S. P. Felix, Studies on Energetic Compounds Part 16: Chemistry and Decomposition Mechanisms of 5-Nitro-2,4-dihydro-3H-1,2,4-triazole-3-one (NTO), *J. Hazard. Mater. B* **2001**, *81*, 67–82.
[3] D. M. Badgujar, M. B. Talawar, S. N. Asthana, P. P. Mahulikar, Advances in Science and Technology of Modern Energetic Materials: An Overview, *J. Hazard. Mater.* **2008,** *151*, 289–305.
[4] M. B. Talawar, R. Sivabalan, T. Mukundan, H. Muthurajan, A. K. Sikder, B. R. Gandhe, A. Subhananda Rao, Environmentally Compatible Next Generation Green Energetic Materials (GEMs), *J. Hazard. Mater.* **2009**, *161,* 589–607.
[5] X. Song, Y. Wang, C. An, X. Guo, F. Li, Dependence of Particle Morphology and Size on the Mechanical Sensitivity and Thermal Stability of Octahydro-1,3,5,7-tetranitro-1,3,5,7-tetrazocine, *J. Hazard. Mater.* **2008**, *159*, 222–229.
[6] D. Spitzer, M. Comet, C. Baras, V. Pichot, N. Piazzon, Energetic Nanomaterials: Opportunities for Enhanced Performances, *J. Phys. Chem. Solids.* **2010**, *71*, 100–108.
[7] R. W. Armstrong, C. S. Coffey, V. F. DeVost, W. L. Elban, Crystal Size Dependence for Impact Initiation for Cyclotrimethylenetrinitramine Explosive, *J. Appl. Phys*. **1990**, *68*, 979–984.
[8] V. Stepanov, V. Anglade, W. A. Balas Hummers, A. V. Bezmelnit *syn*, L. N. Krasnoperov, Production and Sensitivity Evaluation of Nanocrystalline RDX-Based Explosive Compositions, *Propellants Explos. Pyrotech*. **2011**, 36, 240 – 246.
[9] H. Qiu, V. Stepanov, A. R. Di Stasio, T. Chou, W. Y. Lee, RDX-Based Nanocomposite Microparticles for Significantly Reduced Shock Sensitivity, *J. Hazard. Mater.* **2011**, *185*, 489–493.
[10] J. Vágenknecht, P. Mareček, W. A. Trzciński, Sensitivity and Performance Properties of TEX Explosives, *J. Energ. Mater.* **2006**, *20*, 245 – 253.
[11] G. Yang, F. Nie, H. Huang, L. Zhao, W. Pang, Preparation and Characterization of nano-TATB Explosive, *Propellants Explos. Pyrotech.* **2006**, *31*, 390 – 394.
[12] Y. Zhang, D. Liu, C. Lv, Preparation and Characterization of Reticular nano-HMX, *Propellants Explos. Pyrotech.* **2005**, *30*, 438 – 441.
[13] F. Nie, J. Zhang, Q. Guo, Z. Qiao, G. Zeng, Sol-Gel Synthesis of Nanocomposite Crystalline HMX/AP Coated by Resorcinol-Formaldehyde, *J. Phys. Chem. Solids* **2010**, *71*, 109–113.
[14] A. A. Thorat, S. V. Dalvi, Liquid Antisolvent Precipitation and Stabilization of Nanoparticles of Poorly Water Soluble Drugs in Aqueous Suspensions: Recent Developments and Future Perspective, *Chem. Eng. J.* **2012**, *181*, 1–34.
[15] T. M. Tilloston, A. E. Gash, R. L. Simpson, L. W. Hrubesh, J. H. Satcher Jr, J. F. Poco, Nanostructured Energetic Materials Using Sol-Gel Methodologies, *J. Non-Cryst. Solids.* **2001**, *285*, 338 – 345.
[16] Y. Bayat, S. M. Pourmortazavi, H. Iravani, H. Ahadi, Statistical Optimization of Supercritical Carbon Dioxide Antisolvent Process for Preparation of HMX Nanoparticles, *J. Supercrit. Fluids.* **2012**, *72*, 248 – 254.
[17] B-M. Lee, S-J. Kim, B-C Lee, H-S. Kim, H. Kim and Y-W. Lee, Preparation of Micronized β-HMX Using Supercritical Carbon Dioxide as Antisolvent, *Ind. Eng. Chem. Res.* **2011**, *50*, 9107 – 9115.
[18] T. Tsuzuki, P. G. McCormick, Mechanochemical Synthesis of Nanoparticles, *J. Mater. Sci.* **2004**, *39*, 5143 – 5146.
[19] M. N. Patil, G. M. Gore, A. B. Pandit, Ultrasonically Controlled Particle Size Distribution of Explosives: A Safe Method, *Ultrason. Sonochem*. **2008**, *15*, 177–187.
[20] J. Kaur, V. P. Arya, G. Kaur, T. Raychaudhuri, P. Lata, Evaluation of Ultrasonic Treatment for the Size Reduction of HNS and HMX in Comparison to Solvent-Antisolvent Crystallization, *Propellants Explos. Pyrotech*. **2012**, *37*, 662–669.
[21] J. Wang, J. Li, C. An, C. Hou, W. Xu, X. Li, Study on Ultrasound- and Spray-Assisted Precipitation of CL-20, *Propellants Explos. Pyrotech*. **2012**, *37*, 670–675.

[22] N. Radacsi, A. I. Stankiewicz, Y. L. M. Creyghton, A. E. D. M. van der Heijden, J. H. ter Horst, Electrospray Crystallization for High-Quality Submicron-Sized Crystals, *Chem. Eng. Technol.* **2011**, *34*, 624 – 630.

[23] N. Radacsi, A. E. D. M. Van der Heijden, A. I. Stankiewicz, J. H. ter Horst, Cold Plasma Synthesis of High Quality Organic Nanoparticles at Atmospheric Pressure, *J. Nanopart. Res.* **2013**, *15*, 1445.

[24] Y. Dong, W. K. Ng, S. Shen, S. Kim, R. B. H. Tan, Preparation and Characterization of Spironolactone Nanoparticles by Antisolvent Precipitation, *Int. J. Pharm.* **2009**, *375*, 84 – 88.

[25] X. Zhao, K. Song, S. Wang, Y. Zu, N. Li, X. Yu, Micronization of the Pharmaceutically Active Agent Genipin by an Antisolvent Precipitation Process, *Chem. Eng. Technol.* **2013**, *36*, 33 – 42.

[26] Y.-H. Luo, G.-G. Wu, B.-W. Sun, Antisolvent crystallization of Biapenem: Estimation of Growth and Nucleation Kinetics, *J. Chem. Eng. Data* **2013**, *58*, 588–597.

[27] J. M. Vaughn, X. Gao, M.-J. Yacaman, K. P. Johnston, R. O. Williams III, Comparison of Powder Produced by Evaporative Precipitation into Aqueous Solution (EPAS) and Spray Freezing into Liquid (SFL) Technologies Using Novel Z-Contrast STEM and Complimentary Techniques, *Eur. J. Pharm. Biopharm.* **2005**, *60*, 81–89.

[28] X. Chen, T. J. Young, M. Sarkari, R. O. Williams III, K. P. Johnston, Preparation of Cyclosporine A Nanoparticles by Evaporative Precipitation into Aqueous Solution, *Int. J. Pharm.* **2002**, *242*, 3 – 14.

[29] W. E. Bachmann, J. C. Sheehan, A New Method of Preparing the High Explosive RDX, *J. Am. Chem. Soc.* **1949**, *79*, 1842 – 1845.

[30] J. K. Cooper, C. D. Grant, J. Z. Zhang, Experimental and TD-DFT Study of Optical Absorption of Six Explosive Molecules: RDX, HMX, PETN, TNT, TATP, and HMTD, *J. Phys. Chem. A* **2013**, *117*, 6043–6051.

[31] R. E. Schirmer, *Modern Methods of Pharmaceutical Analysis*, CRC Press, Boca Raton, **1991**, p. 34.

[32] H.-B. Fu, J.-N. Yao, Size Effects on the Optical Properties of Organic Nanoparticles, *J. Am. Chem. Soc.* **2001**, *123*, 1434 – 1439.

[33] Y. C. Liau, E. S. Kim, V. Yang, A Comprehensive Analysis of Laser-Induced Ignition of RDX Monopropellant, *Combust. Flame* **2001**, *126*, 1680 – 1698.

[34] E. da Costa Mattos, E. D. Moreira, M. F. Diniz, R. C. L. Dutra, G. D. Silva, K. Iha, U. Teipel, Characterization of Polymer-Coated RDX and HMX Particles, *Propellants Explos. Pyrotech.* **2008**, *33*, 44 – 50.

[35] Z. A. Dreger, Y. M. Gupta, Raman Spectroscopy of High-Pressure High-Temperature Polymorph of Hexahydro-1,3,5-trinitro-1,3,5-triazine (ε-RDX), *J. Phys. Chem. A* **2010**, *114*, 7038–7047.

[36] Z. A. Dreger, Y. M. Gupta, Phase Diagram of Hexahydro-1,3,5-trinitro 1,3,5-triazine Crystals at High Pressures and Temperatures, *J. Phys. Chem. A* **2010**, *114*, 8099–8105.

[37] The Powder Diffraction File, International Centre for Diffraction Data, For RDX: 44-1618, 05-0576, 44-1619 and 44-1606.

[38] G. Singh, S. P. Felix, P. Soni, Studies on Energetic Compounds Part 31. Thermolysis and Kinetics of RDX and Some of its Plastic-Bonded Explosives, *Thermochim. Acta* **2005**, *426*, 131–139.

[39] G. T. Long, S. Vyazovkin, B. A. Breams, C. A. Wight, Competitive Vaporization and Decomposition of Liquid RDX, *J. Phys. Chem. B* **2000**, *104*, 2570 – 2574.

Received: August 13, 2013
Revised: February 20, 2014
Published online: April 6, 2014

